Closed loop motor-sensory dynamics in human vision

Liron Gruber and Ehud Ahissar*

Department of Neurobiology, Weizmann Institute of Science, Rehovot 76100, Israel

*Corresponding Author: ehud.ahissar@weizmann.ac.il

Abstract

Vision is obtained with a continuous motion of the eyes. The kinematic analysis of eye motion, during any visual or ocular task, typically reveals two (kinematic) components: *saccades*, which quickly replace the visual content in the retinal fovea, and *drifts*, which slowly scan the image after each *saccade*. While the saccadic exchange of regions of interest (ROIs) is commonly considered to be included in motor-sensory closed-loops, it is commonly assumed that *drifts* function in an open-loop manner, that is, independent of the concurrent visual input. Accordingly, visual perception is assumed to be based on a sequence of open-loop processes, each initiated by a *saccade*-triggered retinal snapshot. Here we directly challenged this assumption by testing the dependency of *drift* kinematics on concurrent visual inputs using real-time gaze-contingent-display. Our results demonstrate a dependency of the trajectory on the concurrent visual input, convergence of speed to condition-specific values and maintenance of selected *drift*-related motor-sensory controlled variables, all strongly indicative of *drifts* being included in a closed-loop brain-world process, and thus suggesting that vision is inherently a closed-loop process.

Author summary

Our eyes do not function like cameras; it has long been known that we are actively scanning our visual environment in order to see. Moreover, it is commonly accepted that our fast eye movements, *saccades*, are controlled by the brain and are affected by the sensory input. However, our slow eye movements, the ocular *drifts*, are often ignored

when visual acquisition is analyzed. Accordingly, visual processing is typically assumed to be based on computations performed on *saccade*-triggered snapshots of the retinal state. Our work strongly challenges this model and provides significant evidence for an alternative model, a cybernetic one. We show that the dynamics of the ocular *drifts* do not allow, and cannot be explained by, open loop visual acquisition. Instead, our results suggest that visual acquisition is part of a closed-loop process, which dynamically and continuously links the brain to its environment.

Introduction

The visual system usually perceives its environment during egomotion [1-3]. In particular, retinal encoding results from continuous interactions between eye movements and the environment [1, 4-10]. The kinematics of eye movements contain two major motion components: *saccades*, which quickly (speeds between ~10 to ~1000 deg/s) shift the gaze from one region of interest (ROI) to another [11-13] and *drifts*, which slowly (speeds in the order of 1 deg/s) scan each ROI [1, 14-16]. These two kinematic components, *saccades* and *drifts*, fully characterize the movements of the eyes during all kinds of visual activities, whether while fixating, pursuing moving targets, reading or exploring a scene. The faster components, *saccades*, are often divided into macro-*saccades* and micro-*saccades*, depending on their amplitudes. Typically, they shift the gaze to targets beyond or within the foveal field (~1-2 visual degrees at the center of the entire visual field [17], respectively. It is currently accepted that all *saccades* can be characterized along the same kinematic continuum, controlled by the same circuits, and

serve the same function – shifting the gaze to a new ROI [15, 18-22]. Hence, here we analyze all *saccades* in one category.

Two contrasting perceptual schemes might be consistent with this fast-shifts and slow scanning kinematic pattern that dominates primate vision: an open-loop computational and a closed-loop dynamical scheme. In both schemes, *saccades* are controlled, at least in part, in a motor-sensory closed-loop manner, in which ROI selection depends on the accumulated visual information [11, 12, 21, 23-26]. The two schemes, however, divide in their assumed acquisition process in between *saccades*, during what is referred to as *drifts*. The open-loop computational scheme assumes that at each ROI the visual system acquires one snapshot of the ROI per *saccade* and computes its internal representation through an open-ended sequence of computations, much like in current computer-vision implementations [27-31]. The dynamical scheme, in contrast, assumes that the acquisition, and hence also the perception, of each ROI is a continuous closed-loop process, whose dynamics are determined by the interactions between the *drift* motion and the external image [32-36].

As a result, the two schemes entail contrasting predictions. (i) The computational scheme predicts that the ocular *drifts* will not depend on the concurrent visual input, whereas the dynamical scheme predicts that it will. (ii) The dynamical scheme further predicts that the *drifts* will exhibit convergence dynamics during perception (that is, their kinematics should gradually approach steady values during the process), as expected from the dynamics of a closed-loop system around its attractors [36]; the computational scheme predicts that *drifts* dynamics should follow a predetermined or random pattern. (iii) Lastly, with closed-loop perception, adaptive changes are part of a process that attempts

to maintain specific dynamic variables (the “controlled variables”) within specific ranges of values (the “working ranges”) such that perception is optimized [36-38]. Open-loop systems do not have this active capacity and depend on a-priori mapping between environmental and internal variables. Thus, for example, closed-loop perception predicts that oculomotor dynamics will change such that retinal outputs will have temporal characteristics that are optimal for neural processing whereas open-loop perception predicts that such oculomotor changes will reflect motor adaptations such as muscle fatigue.

To test the predictions of the two schemes, we measured ocular behavior while modulating the available spatial information by reducing image size and by mimicking tunnel vision. We tracked subjects’ gaze while they were viewing simple shapes of two sizes, and while revealing to them either the entire visual field (“natural viewing”) or only a portion of the image around the center of their gaze (“tunneled viewing”).

Results

Five subjects were asked to identify an image on a screen as one of five options (square, rectangle, circle, triangle and a parallelogram) after viewing it either naturally or through tunneled viewing, during which spatial information was exposed only around the center of their continuously-tracked gaze. Two image sizes and two tunneling windows were used, with similar ratio between the image and window sizes (10.80±0.15 deg^2 and 0.90±0.03 deg^2 for the large and small shapes; see **Methods,** and Supplementary **Video S1**). Success rates were 100% for natural viewing of both sizes, 94±6% for the tunneled-

large shapes and 60±2% for the tunneled-small shapes. Only correct trials were used for the analyses reported here.

As predicted by both perceptual schemes, limiting the available spatial information had a dramatic effect on gaze locations. During natural viewing of large shapes, the gaze was typically directed around the center of the shape, while during tunneled viewing of large shapes the gaze was typically directed to the borders of the shapes (see examples in **Fig. 1a**). In fact, most (55±7%) of the *saccades* made by all subjects in all tunneled-large trials were border-*saccades*, i.e., started and ended near the border (**Fig. 1b**, see **Methods**).

With tunneled viewing, *saccades* were directed along the image borders (**Fig. 1c** and Supplementary **Fig. S1),** without being able to acquire any information from the target location prior to landing (mean saccadic amplitude was significantly larger than window size, 3.45±0.07 vs 2.90 deg; $p<0.05$, n= 4648, one-tailed t-test; the large tunneling window is overlaid on the rectangle example in **Fig. 1a**). Moreover, saccadic border-following was evident already at the beginning of each trial and, on average, kept a constant profile along the trial (**Fig. 1d**). This suggests that *saccade* planning was primarily based on the information collected during the immediately preceding fixational pause(s) rather than on an accumulated estimation of the object's shape along the trial. Thus, our tunneling results show that target selection can be based on the information actively acquired at the fovea during a single pause without any external, peripheral or foveal, cue.

Figure 1. Eye trajectories. (a) Example of eye trajectories in single trials with natural (left) and tunneled (right) viewing of large shapes. *Saccades*, lighter blue; *drifts*, dark blue; traces, horizontal and vertical components as a function of time next to each example (movies of these examples are in Supplementary **Video S2**). The small yellow rectangle overlaid on the rectangle image shows the window size through which the images were viewed in the tunneled condition. **(b)** Fractions of border *saccades* in the two large-shapes conditions for each subject (small dots) and their means (large dots). **(c)** Distribution of the angles between the orientation of the border scanned during a pause and the direction of the immediately following *saccade* with tunneled large viewing. Purple, empirical data, Gray, shuffled data (*saccade* directions were shuffled before angle computation; average of 100 repetitions is depicted). The histograms of the empirical and shuffled data are superimposed in the graph, and statistically different ($p<0.05$, two-sample Kolmogorov-Smirnov test). Analyses of individual subjects are presented in Supplementary **figure S1-1**. **(d**) Same as (c) for the first, second, third and fourth quarter of each trial. In all four cases, the distributions of the empirical and shuffled data differed significantly ($p<0.05$, two-sample Kolmogorov-Smirnov tests).

To better understand how this information is collected in each pause, we examined the dependency of ocular kinematics on concurrent visual acquisition within each fixational pause. As the exact kinematics of the *drifts* are not directly accessible to current tracking technologies [8, 39], we chose to analyze the lower- and upper-bounds of *drifts* speed. The distributions of our UB (upper-bound) and LB (lower-bound) speeds (**Fig. 2**, blue and cyan, respectively) show higher values than those typically reported in the literature (*40*). To verify that our recordings did not yield higher *drift*s speeds than those previously reported, we replicated the filtering and saccade detection methods reported previously and compared the resulting distribution of our *drift*s speeds (**Fig. 2**, black) with those

previously reported [16]. The comparison reveals that our recording method extract *drifts* speeds of the same distribution as previously reported.

Importantly, our results are based on comparisons between conditions, thus are insensitive to the absolute values of the actual kinematic variables. For clarity, our report is based on the upper-bound speed (UB-speed), where the lower-bound (LB speed) values are described as Supplementary material. Using the UB-speed allows us to estimate the lower bounds of the temporal intervals generated at the retina during *drift* scanning (see **Discussion**).

Figure 2. Bounds of *drifts* kinematics. Distribution of the instantaneous *drift* speeds of all measured fixational pauses of the experiment. Three calculations were used: the upper bound (UB) was assessed by derivation of the raw eye position data, and thus using a higher saccadic detection threshold of 16 deg/s minimal peak velocity and 0.3 deg for minimal amplitude (blue, UB – these are the values reported in this paper). A lower bound (LB, cyan) was assessed by derivation of the filtered eye position data (a third order Savitzky-Golay filter with window size of 3 samples [40]). A comparison to previously published values is presented by thresholding and filtering our data as was previously done (black; filtering as for our lower bound and in addition we used lower saccadic detection thresholds: 3 deg/s for minimal peak velocity and 0.05 deg for minimal amplitude[40].

We first examined the dependency of the scanning patterns of *drifts* on concurrent visual details. Comparing *drifts* in ROIs that did or did not contain borders revealed the following difference. When challenged by tunneling, *drifts* scanning depended on the concurrently scanned visual image - the eye tended to drift in a curvier pattern when

scanning a border, remaining closer to its starting location. The distributions of curvature indexes (see **Methods**) differed between border and non-border *drifts* in both tunneled conditions ($p<0.05$, Kolmogorov–Smirnov test) (**Fig. 3a**). A difference between the mean values was also found in the natural small condition ($p<0.05$, two tailed t-test; **Fig. 3a**), suggesting a similar trend of drift curviness also when the visual system was challenged by small images.

The presence of an image border in the field of view had an immediate effect on additional kinematic variable - the UB-speed of the ocular *drifts* (see **Methods**). The *drifts* UB-speed was significantly lower for border-containing ROIs (**Fig. 3b,** $p<0.05$ in 3 out of the 4 conditions, two tailed t-tests). The viewing condition (natural or tunneled) had an even stronger effect on the *drifts* UB-speed. During tunneled viewing the *drifts* UB-speed was significantly higher than during natural viewing ($p<0.05$, for both image sizes, two tailed t-tests; **Fig. 3b** 1st and 3rd panels versus 2nd and 4th; see also Supplementary **Fig. S**3).

In addition to a dependency on real-time sensory information, the closed-loop scheme also predicts convergence dynamics [36, 41-44]. Indeed, in all our conditions the ocular *drift* UB-speed exhibited a converging-like behavior. On average, consistent with previous observations [45], the *drift* UB-speed was strongly modulated at the beginning of each pause and gradually converged to an asymptotic value during the pause (**Fig. 3b** and Supplementary **Fig. S**3). The convergence to an asymptotic target speed value was evident also for individual subjects, and these target speeds were typically stable for the entire durations of the fixational pauses (Supplementary **Fig. S**3). Importantly, the *drift* UB-speeds we measured did not depend on the pupil size or on the amplitudes or speeds

of the *saccades* preceding them ($r^2 < 0.01$ for all cases), and these variables were not significantly different across viewing conditions (Supplementary **Fig. S2**).

Figure 3. *Drifts* curvature indices and instantaneous UB-speed. **(a)**. Normalized distributions of curvature indices of border *drift*s trajectories (brown) and non-border *drifts* trajectories, in the four experimental conditions. Natural viewing in black and tunneled viewing in color (large in purple and small in green). The vertical lines depict the mean values of curvature indices per condition. Mean ± SEM of the curvature index and the number of pauses for border and non-border scanning, respectively: 0.48±0.04 vs. 0.49±0.01 for natural-large (n=192,374 pauses); 0.52±0.01 vs. 0.48±0.01 for tunneled-large (n=1405,757); 0.65±0.05 vs. 0.55±0.02 for natural-small (n=23,270); 0.60±0.03 vs. 0.53±0.01 for tunneled-small (n=66,2723); p-values in each panel are for (i) comparing means using two tailed t-tests and (ii) comparing distributions using two-sample Kolmogorov-Smirnov tests. **(b)** Mean within-pause instantaneous UB *drifts* speeds of border *drifts* and non-border *drifts*, in the four experimental conditions (colors as in (a)). Mean ± SEM and number of pauses for border and non-border scanning (target speed values, for time>50ms), respectively: 4.64±0.09 vs. 5.14±0.07 for natural-large (n=143,310 pauses); 6.19±0.05 vs. 6.56±0.07 for tunneled-large (n=863,457); 3.9±0.2 vs. 4.81±0.07 for natural-small (n=19,229); 5.9±0.2 vs. 6.20±0.03 for tunneled-small (n=48,1851); (*, p<0.05, two tailed t-tests).

The dependency of ocular kinematics on the concurrent sensory information described so far indicate a closed-loop sensory-motor behavior of the visual system and suggest that the closed-loop processing is done at multiple levels, at least those levels controlling *saccades* and *drifts*. What might the visual system try to maintain using these loops, and in particular during natural and tunneled perceptual epochs? To address these questions, we analyzed the averaged kinematics in each condition per subject. For most subjects, both the *saccades*' mean rate (*Rs*, **Fig. 4a**) and mean target (i.e., for time>50 ms) *drift*

UB-speed per pause (*Sp*, **Fig. 4b***)* increased in tunneled conditions compared to natural viewing. These differences did not result from the differences in trial length (Supplementary **Table S1).** Interestingly, the distance travelled during a pause, the *drift* length or amplitude, (*Xp*), did not change for most subjects (**Fig. 4c).**

Figure 4. Kinematics of *saccades* and *drifts*. (a) Mean saccadic rates (*Rs*) in natural (black) and tunneled viewing for large (purple) and small (green) image sizes. Data for each subject is presented (*, $p<0.05$, two tailed t-tests). **(b)** Distributions of the mean instantaneous UB-speeds of *drifts* (target speed values, for time>50ms) per pause (*Sp*) in the four experimental conditions; data presented as in (a) (*, $p<0.05$, two tailed t-tests). **(c)** Distributions of the distances travelled during a pause (*drift* length; *Xp*) in the four experimental conditions; data presented as in (a) (*, $p<0.05$, two tailed t-tests). N's for *Rs* statistics in tunneled-large, natural-large, tunneled-small, natural-small, respectively, were: Subj1 (30,19,30,20); Subj2 (29,20,30,19); Subj3 (27,20,28,18); Subj4 (30,20,30,19); Subj5 (25,20,30,20); N's for *Sp* and *Xp* statistics were (respectively): Subj1 (127,497,97,259); Subj2 (92,164,35,491); Subj3 (55,195,41,415); Subj4 (60,115,20,286); Subj5 (117,347,53,446).

Assuming that visual information is indeed acquired during fixational pauses [23, 46-49], as expected in a closed-loop scheme, and that photoreceptors are activated by illumination changes, the mean rate of visual acquisition (during a pause) should be proportional to *Sp* [9, 14] and the amount of visual information collected during that pause should be proportional to the integrated distance scanned by the eye (the length of its trajectory) during the pause (*Xp*).

Importantly, on average, the tunneling-induced changes in *Rs* and *Sp* compensated each other, keeping *Xp* unchanged, for each stimulus size (**Fig. 5, Table on top**). Thus, when tunneled, the visual system appeared to increase the ROI sampling rate (*Rs*) while maintaining *Xp* and compromising (i.e., loosening) the control of *Sp*. If the control of *Sp* was indeed loosened, the trial-to-trial variability of *Sp* should increase. Indeed, while *Sp* exhibited relatively small coefficients of variation (CVs) during natural viewing (0.90 and 0.57 for large and small, respectively), its CVs increased significantly when tunneled (1.22 and 1.02 for large and small, respectively; two tailed f-tests, both $p < 0.05$).

Interestingly, a different strategy appeared with size changes. When viewing small sized images, the visual system decreased the ROI sampling rate (consistent with [50]) while maintaining *Sp* and thus increasing *Xp* (**Fig. 5, Table on top**). A sequential open-loop scheme, in which the visual input affects *Rs* and *Rs* affects the *drifts* variables, is ruled out here; the mean values of *Rs* did not systematically change along with either *Sp* or *Xp*, and the pause-by-pause correlations between each *Sp* or *Xp* and its preceding instantaneous *Rs* (i.e., the inter-saccadic-interval) were negligible ($R^2 < 0.06$).

Figure 5. Control variables and closed-loop visual acquisition. (**upper table**) Mean ± SEM of visual scanning variables during each viewing condition (NL, natural large; TL, tunneled large; NS, natural small; TS, tunneled small). *Sp* is the mean instantaneous *drift* speed during a pause in deg/s, *Xp* is the distance travelled during a pause (*drift* length) in deg and *Rs* is the mean saccadic rate per trial. Light blue arrows indicate values that do not differ statistically ($p > 0.15$); all other differences were statistically significant ($p < 0.05$). (**a**) Coordinated *saccade* and *drift* closed-loops. The two loops interact with each other, coordinating the control of the acquisition. (**b**) Controlled variables. The scheme symbolizes the

maintenance of *Sp* across image size (large and small) and the maintenance of *Xp* across viewing conditions (natural and tunneled).

Discussion

Consistent with previous reports [14, 51-56], our results demonstrate clearly that ocular *drifts* are actively controlled by the visual system. What our results add is that this control is part of a motor-sensory closed-loop process: *drifts* kinematics, which affect the visual input, depend on this very same input. We demonstrate this closed-loop behavior via three major observations. First, we showed that the trajectory of the *drift* within each ROI depends on the concurrent visual sensory data. During fixational pauses in which the *drift* scanned an ROI that contained an image border its scanning trajectory was controlled to be slower and curvier than when it scanned a non-border ROI (**Fig. 3a,b**). Second, we showed that the *drift* speed dynamically converges to a condition-specific target speed; even when starting with a speed that was similar for two conditions, in each condition the visual system gradually changed its *drift* speed until it converged, on average, to a value that was specific to that specific viewing condition (**Fig. 3b;** see ***Controlled variables*** below). Third, we found two potential *drift*-related controlled variables - *drift* speed and scanning distance – each affecting the visual information acquired via *drift* motions (**Fig. 5**). Controlled variables are a clear signature of closed-loop systems [37, 44, 57].

These results do not rule out additional contributions to *drifts* control, other than those of the concurrent visual input, such as experience- and context-dependent biases [14, 52, 53] or slow motor-control processes [58]. Under the closed-loop framework, these broader and slower contributions would operate within higher-level sensory-motor loops [21, 36].

Measurement noise and head movements

Our measurements are contaminated with measurement noise. With video-based methods, such as the one we used, the major noise sources are inaccurate calibration, slow changes in the pupil size and head movements [59-61]. Importantly, however, pupillary responses to changes in the visual input exhibit significantly slower dynamics than those shown here [62]. Moreover, our results are based on comparisons between conditions, and we used the exact same methods in all conditions. We thus ruled out the possibility that the differences we found stemmed from differences in pupil size (Supplementary **Fig. S2**) or insufficient calibration (we calibrated the device before each trial – see **Methods**) between conditions. Head movements most likely cannot account for the rapid kinematics demonstrated in **Fig. 3** [63, 64]. We remain with a possible contribution of head movements to the slow kinematics; thus, it is possible that part of the differences we measured in the slow kinematics of the *drifts* are in fact differences in the kinematics of head movements. However, importantly, this possibility has no effect on our major conclusion that visual acquisition is a closed-loop motor-sensory process. Since head movements always contribute to retinal image-motion [1, 51, 64, 65], whether retinal motion was controlled in a closed-loop manner in our experiment via *drifts* alone or via *drifts* + head motion makes no difference in this respect.

The exact value of the *drift* speed is not directly accessible to current tracking technologies [8, 39]. We thus assessed the upper and lower bounds (UB and LB, respectively) of the instantaneous *drift* speed by analyzing the unfiltered and filtered tracking data, respectively [16]. We also verified that our recording method generates measures of eye speed that are similar to those obtained in previous studies with other

methods (see **Fig. 2** and related text). Assuming that the recording noise was similar across the different conditions, comparing ocular kinematics across conditions should yield the same results whether based on the upper or lower bounds. Indeed, this was the case here **(e.g.,** Supplementary **Fig. S2)**. It should be emphasized here, again, that since all our conclusions are based on comparisons of the same measures across conditions, our conclusions are insensitive to the absolute values of the actual kinematic variables.

Drift convergence and post-saccadic enhancement

Saccades are typically followed by a short period of relatively high speed drift, termed post-saccadic enhancement [45, 66]. These periods are associated with periods of enhanced neuronal activity in the brainstem oculomotor nuclei, a phenomenon that was termed pulse-step motor command: a strong initial pulse of action potentials that rapidly moves the eye at saccadic velocities, and a subsequent tonic discharge (step command) that maintains the eye at the saccade endpoint [45, 67]. Our results suggest that this initial boost of drift speed is the beginning of a convergence process, a process through which the oculomotor system converges upon a target *drift* speed that fits the characteristics of the current condition (e.g., the amount of available visual information, as implied here by the difference in target speeds between natural and tunneled viewing conditions; **Fig. 3b**). Such an initial boost may be advantageous for a rapid convergence process, as it dictates the direction of convergence – always decreasing *drift* speed. In any case, our observation that the drift speed converges to condition-dependent and saccade-amplitude-independent speed strongly suggest that the process that stabilizes the *drift* speed is not merely a passive attenuation of brainstem oculomotor activity.

We showed here that the system converges to its target speed within < 100 ms on average (**Fig. 3a**). Such a rapid convergence can only be achieved in loops with cycle times that are significantly smaller than the convergence time – in the visual system these are low-level (certainly sub cortical; [68]) loops. These loops, thus, necessarily involve components that are already known to control saccades [69-71] and smooth pursuit [72] eye movements. Which components are shared across these control functions [73] and which are not is an exciting open question.

Controlled variables

Our data suggest that under normal conditions the visual system controls its *drift* speed such as to maintain it within a specific range [see also [41]]. One plausible reason for such a control is to maintain temporal coding within a range suitable for neural processing [8, 21, 44, 74, 75]. When viewing small-size images, the visual system did not compromise this control, possibly for maintaining the reliability of sensory data. However, when challenged with tunneled viewing, which decreases the amount of available spatial information, the visual system compromised the control of *drift* speed, allowing its increase, for maintaining constant scanning distances under an increased rate of ROI switching (shorter fixational pauses), thus increasing total spatial information (**Fig. 5**).

Temporal coding is forced in active sensing. The movements of the eye convert external spatial information (spatial offsets) to temporal information (temporal offsets, i.e., delays) at the output of the retina [8, 9, 76]. The faster the movement of the eye the larger the amount of information coded in a given period, but also the smaller the characteristic

temporal delays. Typical mammalian neuronal circuits are limited in their ability to follow or decode temporal delays that are smaller than 1 ms [74, 76, 77]. The temporal inter-receptor delays expected when scanning individual edges are equal the inter-receptor spacing divided by the drift speed [21]. Thus, assuming foveal densities of up to 166 photoreceptors per deg [78, 79], inter-receptor temporal delays were likely approaching 1 ms on average ($\frac{\frac{1}{166}\ [deg]}{\sim 5\ [\frac{deg}{sec}]} = \sim 0.001\ [sec]$).

The dependencies observed here suggest that if the acquisition system indeed functions as a closed loop, one of its controlled variables would likely be the minimal temporal delay among its foveal ganglion cells. If this is the case, inverse relationships between its motor-sensory variables are expected. The most reasonable closed-loop scheme, according to our data, is a one in which the bottom-up arc implements the dependency of *Rs* on *Xp*, and the top-down one the dependency of *Xp* on *Rs*. Thus, saccadic ROI switching, which is controlled by both global scene- and task-related factors [5, 11, 12, 15, 20, 80, 81] and local ROI-specific factors [15, 21], appears to be controlled in coordination with the control of the ocular *drift*. We further show here that this coordination is manifested in real time on a cycle-by-cycle basis (**Fig. 1c,d**).

In our paradigm, the coordinated *saccade-drift* control maintained, on average, *Sp* across image sizes in natural viewing, and *Xp* across viewing conditions (**Fig. 5**). The identification of these controlled variables was possible only at the population level, and not with individual subjects. This is not surprising, given the complexity of the human visual system and its need to cope with many changing conditions in life. These results,

thus, suggest that *Sp* and *Xp* are controlled in most of the individual subjects in the manner described above, as part of a larger set of idiosyncratic controlled variables.

Conclusions

That visual information is acquired continuously along each fixational pause had been demonstrated previously [23, 46-49]. Our results now provide substantial evidence that this acquisition is accomplished by retino-neuro-oculo closed-loops, involving low (certainly subcortical) levels of the visual system. Together with the known closed-loop basis of ROI selection, our results now suggest that vision is inherently a closed-loop process. That is, that all visual processing components are accomplished within brain-environment closed-loops. Being inherently a closed-loop system does not preclude the ability of the visual system to perceive a certain amount of information even when eye movements are prevented, as often occurs in the laboratory. Being a closed-loop system simply entails, in this context, that every movement of the eye is a component of visual perception and that the system continuously attempts to converge to its attractors, getting as close to a given attractor as possible, given the collection of internal and external constrains.

Methods

Subjects. 5 healthy subjects with normal vision at the ages 21-28 participated in the experiments (3 females, 2 with right dominant eye, 3 with left dominant eye). All subjects were given detailed explanation about the eye tracker device and the behavioral task, and were paid for their participation. Informed consents were obtained from all

subjects, in accordance with the approved Declaration of Helsinki for this project. The experimental procedures were approved by the Tel Aviv Sourasky Medical Center Helsinki committee.

Experimental Setup. The experiment took place in a darkened and quiet room where subjects sat in front of a high-resolution, fast computer screen (VPixx, 1920x1080, 120Hz). The movements of the dominant eye were recorded using EyeLink II at 100Hz (enabling real time screen manipulation after each sample) while the other eye was blindfolded. Subjects sat 1 meter away from the screen and placed their chin on a chinrest to reduce head movements.

Stimuli and gaze windows. Two kinds of images were created: 'large' and 'small', and each was associated with a specific gaze window – a horizontal rectangle centered on the subject's gaze at each sample and through which the image was exposed. The large shapes occupied 10.80±0.15x10.80±0.15 deg (720±10x720±10 pixels), and the large gaze window was 2.90±0.15x1.90±0.15 deg (190±10x130±10 pixels). The small shapes occupied 0.90±0.03x0.90±0.03 deg (60±2x60±2 pixels) with a gaze window of 0.24±0.03x0.16±0.03 deg (13±2x9±2 pixels). The ratio between image and window size was the same for both image sizes (Supplementary **Video S1**).

Experimental Design. We tested the performance of subjects in a five forced choice shapes recognition tasks. In each trial, one out of five filled gray basic shapes against a black background was presented (square, rectangle, circle, triangle and a parallelogram; see **Fig. 1a**). These images were presented in two forms, large and small, as described above. Subjects were tested during 5 days. During days 1-3 they performed 2 tunneled

vision sessions, the first one with large images and the second one with small images. On day 4 they performed two additional tunneled vision sessions with small images. On day 5 they performed 4 sessions of natural viewing, 2 repetitions with each image size: large, small, large, and small (natural trials were only performed after all tunneled trials ended, to avoid familiarity with the shapes). Each tunneled trial lasted up to 30 s, mean trial duration for tunneled large was 9+2 s and for tunneled small 20+4 s (trials with natural viewing lasted 3 s, hence all comparative analyses were further verified using only the first 3 s of all tunneled trials, to control for trial length confounds, Supplementary **Table S1**). There were at least 2 repetitions of each shape in each session (10-12 trials per session, only the first two repetitions of each shape were used for analysis), and hence each session lasted up to 12 minutes. Before the beginning of each trial the eye tracker was recalibrated [60]. We used an adaptive calibration method: subjects fixated on a '+' and waited until the gaze report of the eye tracker (marked as 'X') stabilized. The error between the two markers was used to correct the eye tracker's output during the next trial. At the end of each trial subjects reported which of the five shapes was presented, and received a 'correct/wrong' feedback. In the tunneled vision sessions, subjects had to identify a shape that was "hidden" on the screen and exposed only through the gaze window (see above). In the natural vision sessions, subjects had to identify the same shapes, naturally viewing them with no constrains.

Eye movement processing. A velocity based algorithm [modified from Bonneh et al. [82]] was used for detecting all *saccades* and *drifts*. We used the following threshold parameters for *saccades* detection: 16 deg/s minimal peak velocity and 0.3 deg minimal amplitude. Each detected *saccade* was visually examined to verify the quality of saccadic

detection. Fixation periods between *saccades* were labeled *drifts* only if they lasted > 30 ms. Upper bounds of the instantaneous *drift* speed were computed as the derivative of the raw eye position signal (100Hz)[16]. Lower bounds were computed as derivatives of the filtered signals (a third order Savitzky-Golay filter with window size of 3 samples [40]). For **Fig. 2** we in addition used saccadic detection threshold parameters of 3 deg/s for minimal peak velocity and 0.05 deg for minimal amplitude, in order to match and compare previous publications [40].

Borders analysis. Border-following movements during tunneled viewing were those movements in which the border of the shape was visible to the subject during the movement. This was determined by the window size: *saccades* or *drifts* pauses that started and ended at less than 1.8 deg (for large), or 0.15 deg (for small) from a border, were classified as "border *saccade*" or "border *drift*", respectively. During natural viewing border-following movements were defined using the same distance criteria.

Curvature index. We defined an index for *drift* curvature, where *Xp* equals the length of the *drift* trajectory and *Dp* equals the linear distance between its starting and ending points. Hence, c=0 represents a straight line and c=1 represents a closed curve.

Statistical analyses. Two-tailed t-tests were used to evaluate the significance of differences in the mean values of kinematic variables (*Rs*, *Sp*, *Xp*, *c*), all of which exhibited normal distribution for all subjects. N's for *Rs* statistics in tunneled-large, natural-large, tunneled-small, natural-small, respectively, were: Subj1 (30,19,30,20); Subj2 (29,20,30,19); Subj3 (27,20,28,18); Subj4 (30,20,30,19); Subj5 (25,20,30,20); N's for *Sp* and *Xp* statistics were (respectively): Subj1 (1756,229,2392,154); Subj2

(534,110,2626,45); Subj3 (723,129,2108,101); Subj4 (409,104,1288,46); Subj5 (1085,203,2775,136).; Distributions of values were also compared using two-sample Kolmogorov-Smirnov tests. Variances were compared via the corresponding coefficients of variation (CV = variance/mean), using two-sample F-tests. Data are expressed as mean ± S.E.M. Shape presentation order was randomized using a uniform distribution. No blinding was done during analysis and none of the data points was excluded.

Acknowledgements

We thank Amos Arieli for his invaluable help in performing the experiments, Ziad Hafed and Laurent Perrinet for their insightful and helpful comments, and Michele Rucci and Rafi Malach for commenting on earlier versions of the manuscript.

References

1. Steinman RM, Levinson JZ. The role of eye movement in the detection of contrast and spatial detail. In: Kowler E, editor. Eye Movements and Their Role in Visual and Cognitive Processes. Amsterdam: Elsevier; 1990. p. 115-212.
2. Keller GB, Bonhoeffer T, Hubener M. Sensorimotor mismatch signals in primary visual cortex of the behaving mouse. Neuron. 2012;74(5):809-15. Epub 2012/06/12. doi: 10.1016/j.neuron.2012.03.040. PubMed PMID: 22681686.
3. Dadarlat MC, Stryker MP. Locomotion Enhances Neural Encoding of Visual Stimuli in Mouse V1. The Journal of Neuroscience. 2017;37(14):3764-75. doi: 10.1523/jneurosci.2728-16.2017.
4. Barlow HB. Eye movements during fixation. J Physiol. 1952;116:290-306.
5. Yarbus AL. Eye Movements and Vision. New York: Plenum; 1967.
6. Noton D, Stark L. Eye movements and visual perception. Sci Am. 1971;224(6):35-43. PubMed PMID: 5087474.
7. Ditchburn RW. Eye-movements and visual perception. Oxford: Clarendon press; 1973.
8. Rucci M, Ahissar E, Burr D. Temporal coding of visual space. Trends in cognitive sciences. 2018;22(10):883-95.
9. Ahissar E, Arieli A. Figuring space by time. Neuron. 2001;32:185-201. doi: DOI: http://dx.doi.org/10.1016/S0896-6273(01)00466-4.
10. Leszczynski M, Schroeder CE. The Role of Neuronal Oscillations in Visual Active Sensing. Frontiers in integrative neuroscience. 2019;13.
11. Noton D, Stark L. Scanpaths in eye movements during pattern perception. Science. 1971;171(968):308-11. PubMed PMID: 5538847.
12. Yang SC-H, Lengyel M, Wolpert DM. Active sensing in the categorization of visual patterns. Elife. 2016;5.
13. Meermeier A, Gremmler S, Lappe M. The influence of image content on oculomotor plasticity. Journal of vision. 2016;16(8):17-.
14. Rucci M, Victor JD. The unsteady eye: an information-processing stage, not a bug. Trends in Neurosciences. 2015;38:195-206.
15. Krauzlis RJ, Goffart L, Hafed ZM. Neuronal control of fixation and fixational eye movements. Phil Trans R Soc B. 2017;372(1718):20160205.
16. Ahissar E, Ozana S, Arieli A. 1-D Vision: Encoding of Eye Movements by Simple Receptive Fields. Perception. 2015;44(8-9):986-94.
17. Rossi EA, Roorda A. The relationship between visual resolution and cone spacing in the human fovea. Nature neuroscience. 2010;13(2):156-7.
18. Zuber BL, Stark L, Cook G. Microsaccades and the velocity-amplitude relationship for saccadic eye movements. Science. 1965;150(3702):1459-60.
19. Rolfs M, Kliegl R, Engbert R. Toward a model of microsaccade generation: The case of microsaccadic inhibition. Journal of vision. 2008;8(11):5.
20. Ko HK, Poletti M, Rucci M. Microsaccades precisely relocate gaze in a high visual acuity task. Nature neuroscience. 2010;13(12):1549-53. Epub 2010/11/03. doi: nn.2663 [pii]

10.1038/nn.2663. PubMed PMID: 21037583.
21. Ahissar E, Arieli A, Fried M, Bonneh Y. On the possible roles of microsaccades and drifts in visual perception. Vision research. 2014;118:25-30.

22. Willeke KF, Tian X, Buonocore A, Bellet J, Ramirez-Cardenas A, Hafed ZM. Memory-guided microsaccades. Nature communications. 2019;10(1):1-14.
23. Wolf C, Schütz AC. Trans-saccadic integration of peripheral and foveal feature information is close to optimal. Journal of vision. 2015;15(16):1-.
24. Shen K, Paré M. Predictive Saccade Target Selection in Superior Colliculus during Visual Search. The Journal of Neuroscience. 2014;34(16):5640-8.
25. Friston K, Adams R, Perrinet L, Breakspear M. Perceptions as hypotheses: saccades as experiments. Frontiers in Psychology. 2012;3. doi: 10.3389/fpsyg.2012.00151.
26. Wang X, Zhang M, Cohen IS, Goldberg ME. The proprioceptive representation of eye position in monkey primary somatosensory cortex. Nature neuroscience. 2007;10(5):640-6.
27. Crick FHC, Marr DC, Poggio T. An information-processing approach to understanding the visual cortex. In: Schmitt FO, editor. The organization of the cerebral cortex. Cambridge: MIT Press; 1981. p. 505-33.
28. Treisman AM, Gelade G. A feature-integration theory of attention. Cognit Psychol. 1980;12(1):97-136.
29. Pitkow X, Sompolinsky H, Meister M. A neural computation for visual acuity in the presence of eye movements. PLoS Biol. 2007;5(12):e331. Epub 2007/12/29. doi: 07-PLBI-RA-0769 [pii]

10.1371/journal.pbio.0050331. PubMed PMID: 18162043; PubMed Central PMCID: PMC2222970.
30. Poggio T, Serre T. Models of visual cortex. Scholarpedia. 2013;8(4):3516.
31. Cadieu CF, Hong H, Yamins DL, Pinto N, Ardila D, Solomon EA, et al. Deep neural networks rival the representation of primate IT cortex for core visual object recognition. PLoS computational biology. 2014;10(12):e1003963.
32. Uexkull Jv. Theoretical biology. London: K. Paul, Trench, Trubner & co. ltd; 1926.
33. Powers WT. Feedback: beyond behaviorism. Science. 1973;179(71):351-6. PubMed PMID: 4682961.
34. Van Gelder T, Port RF. It's about time: An overview of the dynamical approach to cognition. Mind as motion: Explorations in the dynamics of cognition. 1995;1:43.
35. Kelso JS. Dynamic patterns: The self-organization of brain and behavior: MIT press; 1997.
36. Ahissar E, Assa E. Perception as a closed-loop convergence process. eLife. 2016;5:e12830. doi: http://dx.doi.org/10.7554/eLife.12830.
37. Marken RS. You say you had a revolution: Methodological foundations of closed-loop psychology. Review of General Psychology. 2009;13(2):137.
38. Buckley CL, Toyoizumi T. A theory of how active behavior stabilises neural activity: Neural gain modulation by closed-loop environmental feedback. PLoS computational biology. 2018;14(1):e1005926.
39. Fang Y, Gill C, Poletti M, Rucci M. Monocular microsaccades: Do they really occur? Journal of vision. 2018;18(3):1-14.
40. Cherici C, Kuang X, Poletti M, Rucci M. Precision of sustained fixation in trained and untrained observers. Journal of vision. 2012;12(6):31. Epub 2012/06/26. doi: 10.1167/12.6.31. PubMed PMID: 22728680.
41. Biswas D, Arend LA, Stamper SA, Vágvölgyi BP, Fortune ES, Cowan NJ. Closed-Loop Control of Active Sensing Movements Regulates Sensory Slip. bioRxiv. 2018:366609.

42. Saig A, Gordon G, Assa E, Arieli A, Ahissar E. Motor-sensory confluence in tactile perception. The Journal of Neuroscience. 2012;32(40):14022-32. doi: 10.1523/JNEUROSCI.2432-12.2012. PubMed PMID: 23035109.
43. Horev G, Saig A, Knutsen PM, Pietr M, Yu C, Ahissar E. Motor-sensory convergence in object localization: a comparative study in rats and humans. Philosophical transactions of the Royal Society of London Series B, Biological sciences. 2011;366(1581):3070-6. doi: 10.1098/rstb.2011.0157. PubMed PMID: 21969688.
44. Saraf-Sinik I, Assa E, Ahissar E. Motion Makes Sense: An Adaptive Motor-Sensory Strategy Underlies the Perception of Object Location in Rats. The Journal of Neuroscience. 2015;35(23):8777-89.
45. Chen C-Y, Hafed ZM. Postmicrosaccadic enhancement of slow eye movements. Journal of Neuroscience. 2013;33(12):5375-86.
46. Burr DC. Temporal summation of moving images by the human visual system. ProcRSocLondBBiolSci. 1981;211:321-39.
47. Watt R. Scanning from coarse to fine spatial scales in the human visual system after the onset of a stimulus. JOSA A. 1987;4(10):2006-21.
48. Rucci M, Iovin R, Poletti M, Santini F. Miniature eye movements enhance fine spatial detail. Nature. 2007;447(7146):851-4. Epub 2007/06/15. doi: nature05866 [pii]

10.1038/nature05866. PubMed PMID: 17568745.
49. Grill-Spector K, Kanwisher N. Visual recognition: As soon as you know it is there, you know what it is. Psychological Science. 2005;16(2):152-60.
50. Hafed ZM, Goffart L. Gaze direction as equilibrium: more evidence from spatial and temporal aspects of small-saccade triggering in the rhesus macaque monkey. Journal of Neurophysiology. 2020;123(1):308-22.
51. Martinez-Conde S, Macknik SL, Hubel DH. The role of fixational eye movements in visual perception. nature reviews neuroscience. 2004;5(3):229-40. PubMed PMID: 14976522.
52. Rolfs M. Microsaccades: small steps on a long way. Vision research. 2009;49(20):2415-41.
53. Herrmann CJ, Metzler R, Engbert R. A self-avoiding walk with neural delays as a model of fixational eye movements. Scientific Reports. 2017;7(1):12958.
54. Kagan I. Active vision: fixational eye movements help seeing space in time. Current biology : CB. 2012;22(6):R186-8. Epub 2012/03/24. doi: 10.1016/j.cub.2012.02.009. PubMed PMID: 22440800.
55. Intoy J, Rucci M. Finely tuned eye movements enhance visual acuity. Nature Communications. 2020;11(1):1-11.
56. Ağaoğlu MN, Chung ST. Exploration of the functional consequences of fixational eye movements in the absence of a fovea. Journal of vision. 2020;20(2):12-.
57. Marken RS. Controlled variables: Psychology as the center fielder views it. The American Journal of Psychology. 2001;114(2):259.
58. Kowler E, Steinman RM. The effect of expectations on slow oculomotor control. I. Periodic target steps. Vision research. 1979;19(6):619-32.
59. Drewes J, Zhu W, Hu Y, Hu X. Smaller is better: Drift in gaze measurements due to pupil dynamics. PloS one. 2014;9(10):e111197.
60. Nyström M, Andersson R, Holmqvist K, Van De Weijer J. The influence of calibration method and eye physiology on eyetracking data quality. Behavior research methods. 2013;45(1):272-88.

602 61. Ko H-k, Snodderly DM, Poletti M. Eye movements between saccades: Measuring ocular
603 drift and tremor. Vision research. 2016;122:93-104.
604 62. Clarke RJ, Zhang H, Gamlin PD. Characteristics of the pupillary light reflex in the alert
605 rhesus monkey. Journal of Neurophysiology. 2003;89(6):3179-89.
606 63. Skavenski A, Hansen R, Steinman RM, Winterson BJ. Quality of retinal image stabilization
607 during small natural and artificial body rotations in man. Vision research. 1979;19(6):675-83.
608 64. Poletti M, Aytekin M, Rucci M. Head-eye coordination at a microscopic scale. Current
609 Biology. 2015;25(24):3253-9.
610 65. Gilchrist ID, Brown V, Findlay JM. Saccades without eye movements. Nature.
611 1997;390(6656):130-1.
612 66. Kawano K, Miles F. Short-latency ocular following responses of monkey. II. Dependence
613 on a prior saccadic eye movement. Journal of neurophysiology. 1986;56(5):1355-80.
614 67. Van Gisbergen J, Robinson DA, Gielen S. A quantitative analysis of generation of saccadic
615 eye movements by burst neurons. Journal of Neurophysiology. 1981;45(3):417-42.
616 68. Schmolesky MT, Wang Y, Hanes DP, Thompson KG, Leutgeb S, Schall JD, et al. Signal
617 timing across the macaque visual system. Journal of neurophysiology. 1998;79(6):3272-8.
618 69. Robinson D. The use of control systems analysis in the neurophysiology of eye
619 movements. Annual review of neuroscience. 1981;4(1):463-503.
620 70. Fuchs A, Kaneko C, Scudder C. Brainstem control of saccadic eye movements. Annual
621 review of neuroscience. 1985;8(1):307-37.
622 71. Coe BC, Munoz DP. Mechanisms of saccade suppression revealed in the anti-saccade
623 task. Philosophical Transactions of the Royal Society B: Biological Sciences.
624 2017;372(1718):20160192.
625 72. Behling S, Lisberger SG. Different mechanisms for modulation of the initiation and
626 steady-state of smooth pursuit eye movements. Journal of Neurophysiology. 2020;123(3):1265-
627 76.
628 73. Keller EL, Missal M. Shared brainstem pathways for saccades and smooth-pursuit eye
629 movements. 2003.
630 74. Ahissar E. Temporal-code to rate-code conversion by neuronal phase-locked loops.
631 Neural Comput. 1998;10(3):597-650.
632 75. Ahissar E, Arieli A. Seeing via miniature eye movements: A dynamic hypothesis for
633 vision. Frontiers in Computational Neuroscience. 2012;6:89. doi: 10.3389/fncom.2012.00089.
634 76. Meister M, Berry MJ, 2nd. The neural code of the retina. Neuron. 1999;22(3):435-50.
635 PubMed PMID: 10197525.
636 77. Jones LM, Depireux DA, Simons DJ, Keller A. Robust temporal coding in the trigeminal
637 system. Science. 2004;304(5679):1986-9. PubMed PMID: 15218153.
638 78. Curcio CA, Sloan KR, Kalina RE, Hendrickson AE. Human photoreceptor topography.
639 Journal of comparative neurology. 1990;292(4):497-523.
640 79. Roorda A, Romero-Borja F, Donnelly III WJ, Queener H, Hebert TJ, Campbell MC.
641 Adaptive optics scanning laser ophthalmoscopy. Optics express. 2002;10(9):405-12.
642 80. Findlay JM, Brown V. Eye scanning of multi-element displays: II. Saccade planning. Vision
643 research. 2006;46(1-2):216-27. PubMed PMID: 16169036.
644 81. Schütz AC, Braun DI, Gegenfurtner KR. Eye movements and perception: A selective
645 review. Journal of vision. 2011;11(5):9-.
646 82. Bonneh YS, Donner TH, Sagi D, Fried M, Cooperman A, Heeger DJ, et al. Motion-induced
647 blindness and microsaccades: cause and effect. Journal of vision. 2010;10(14):22.

648

Supplementary information captions

Video S1. Demonstrations of tunneled viewing. Movies of tunneled viewing of large (top) and small (bottom) shapes. The right panels show the entire shape with the tunneling window superimposed and the left panels show what was presented on the screen.

Videos S2. Demonstrations of the eye trajectories presented in Fig. 1. Movie is slowed down by 2.4. Colors as in Fig 1. In addition, black segments represent an un-classified movement along the trial (e.g., pauses shorter than 40ms).

Table S1. Control for trial duration differences. Related to Figure 4. The analyses described in **Fig. 3** were repeated for the first 3 s of the tunneled conditions, a time period equal to the duration of natural viewing trials. P values represent the probability that the values measured in the relevant tunneled condition were drawn from the same distribution as those measured in the natural viewing conditions (two tailed t-tests for means and two tailed f-tests for variances).

Figure S1. *Saccades* direction following border scanning. Related to Figure 1bc. Distributions of the angles between the orientation of the border scanned during a pause and the direction of the immediately following *saccade* [data shown in purple, shuffled data (*saccade* directions were shuffled before angle computation; average of 100 repetitions is depicted) in gray]. Data for each is presented. All distributions are statistically different, $p<0.05$, two-sample Kolmogorov-Smirnov tests.

Figure S2. Dependencies between kinematic variables. Related to Figure 3**. (a)** The mean amplitude of the preceding *saccades* of all pauses in each of the four experimental conditions; no significant difference was found ($p > 0.1$, two-tailed t-test); similarly, no significant difference was found for the maximal *saccade* speed ($p > 0.1$, two-tailed t-test). **(b-d)** Each data point represents a single pause (mean pause

speed versus (b) the amplitude of the preceding *saccade*, (c) the maximal speed of the preceding *saccade* (d) mean pupil size during the pause). $R^2 < 0.01$ in all cases. Colors as in Fig. 3. **(e)** Mean within-pause instantaneous pupil size **(f)** Mean within-pause instantaneous *drift* speed (no correlation with the mean within-pause instantaneous pupil size, $R^2 = 0.02$, $p = 0.55$) **(g)** Lower bound of the mean within-trial instantaneous *drift* speed, calculated from the filtered data (a third order Savitzky-Golay filter with window size of 3 samples [40]).

Figure S3. Stability of instantaneous *drift* speed convergence. Related to Figure 3. **(a)** Mean within-pause instantaneous *drift* speeds presented for large (left) and small (right) objects, depicted for $0<t<100$ ms from pause onset (colors as in Fig. 3). Error-bars denote SEMs across pauses. Light colors show individual means per subject. **(b)** same as (a) for $0<t<400$ ms.

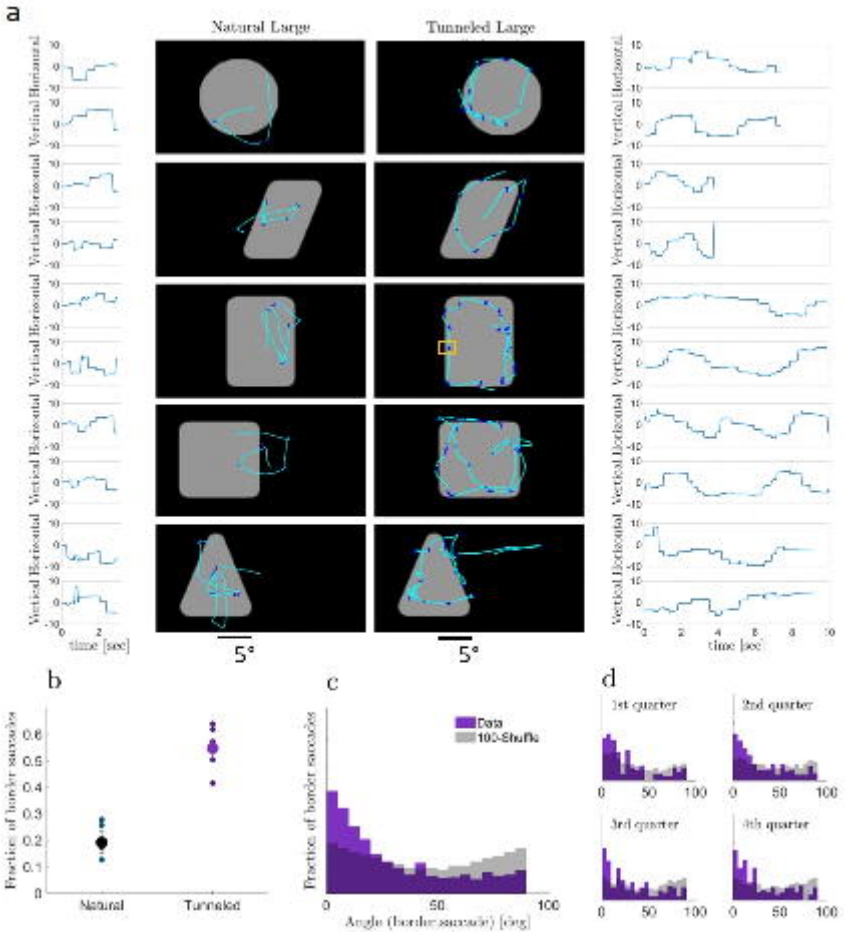
a
Natural Large
Tunneled Large
Vertical
Horizontal
time [sec]
5°
5°
b
Fraction of border saccades
Natural
Tunneled
c
Data
100-Shuffle
Fraction of border saccades
Angle (border saccade) [deg]
d
1st quarter
2nd quarter
3rd quarter
4th quarter

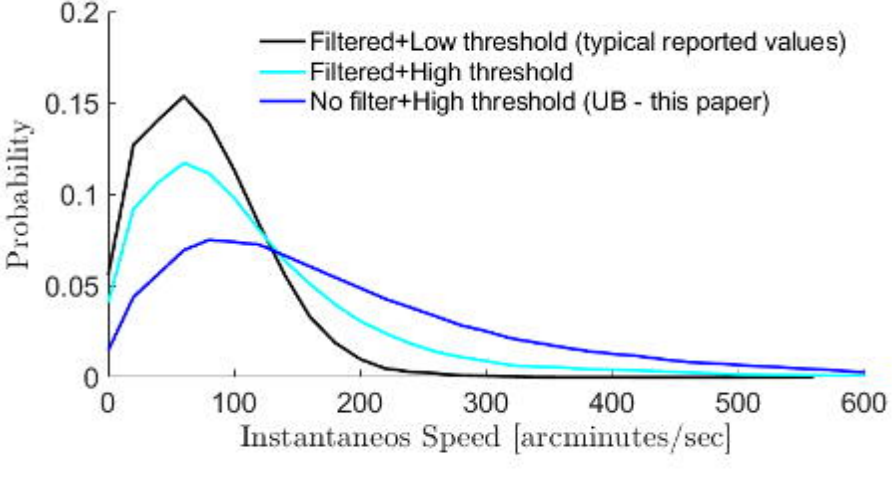
Filtered+Low threshold (typical reported values)
Filtered+High threshold
No filter+High threshold (UB - this paper)
Probability
0.2
0.15
0.1
0.05
0
0
100
200
300
400
500
600
Instantaneos Speed [arcminutes/sec]

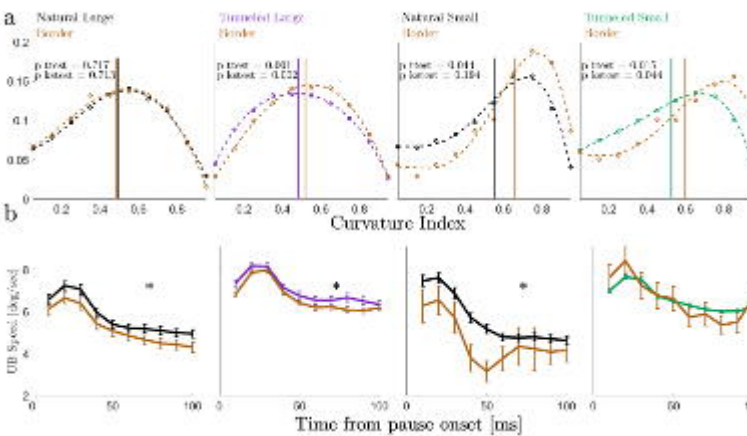
a
Natural Large
Turneted Large
Natural Small
Turneted Small
Curvature Index
b
Time from pause onset [ms]

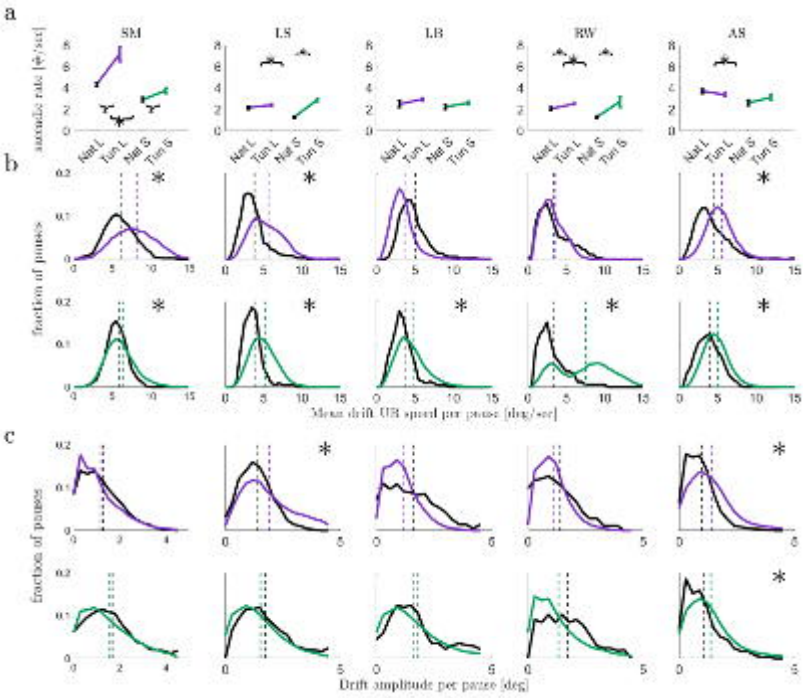
a
SM
LS
LB
RW
AS
saccade rate [#/sec]
Nat L
Tun L
Nat S
Tun S
b
fraction of pauses
Mean drift UB speed per pause [deg/sec]
c
fraction of pauses
Drift amplitude per pause [deg]

	Sp	*Xp*	*Rs*
NL	4.89±0.09	1.33±0.04	2.9±0.1
TL	5.81±0.05	1.40±0.04	3.7±0.2
NS	4.56±0.09	1.77±0.08	2.0±0.1
TS	5.60±0.03	1.63±0.08	3.0±0.1

a. Closed-loop acquisition

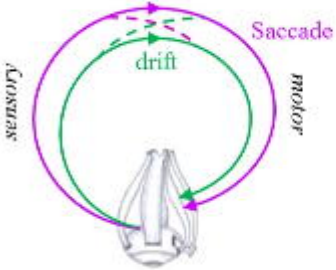
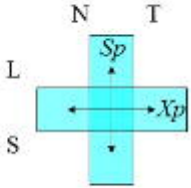
b. Controlled variables